Journal of Hydrology 593 (2021) 125810

Contents lists available at ScienceDirect

Journal of Hydrology

journal homepage: www.elsevier.com/locate/jhydrol

Research papers

Time lapse electric resistivity tomography to portray infiltration and hydrologic flow paths from surface to cave

Matthias Leopold [a,*], Conrad Gupanis-Broadway [a], Andy Baker [b,c], Stuart Hankin [c], Pauline Treble [c,b]

[a] UWA School of Agriculture and Environment, Soil Matrix Group, University of Western Australia, 6009 Perth, Australia
[b] Connected Waters Initiative, UNSW Sydney, Sydney 2052, Australia
[c] ANSTO, Lucas Heights 2234, Australia

ARTICLE INFO

This manuscript was handled by Corrado CorradiniIn, Editor-in-Chief, with the assistance of Junbing Pu, Associate Editor

Keywords:
Electric resistivity tomography (ERT)
Cave monitoring
Karst hydrology
Karst critical zone
ERT-hydrogeological zone

ABSTRACT

This study provides the example of Golgotha Cave, in the south west of Western Australia, where previous long-term hydrological, geochemical and climate monitoring resulted in a theoretical hydrological model of the karst critical zone. We test this model by presenting the results of a 1.5 year monitoring program above the cave using time-lapse electric resistivity tomography (TL-ERT). Between May 2016 and January 2018 several lines up to 200 m long were monitored using a 100 multi-electrode Lipmann 4point light instrument. Various Wenner and Dipole-Dipole arrays provided information of electric resistivity changes at certain points of the year. Laboratory studies measuring volumetric water content versus electric resistivity of various rocks and soils resulted in three different ERT-hydrogeological zones. Besides the annual infiltration patterns, TL-ERT also identified previously unknown, permanent water storages as well as several areas acting as fast hydrological flow pathways most likely caused by pipe structures in the aeolianite. Specific aspects of the TL-ERT study could be correlated with the long term drip water monitoring and thus confirmed and extended the hydrogeological model of the area. A resulting conceptual model of the flow pathways derived from ERT surveys and cave water monitoring results is presented to visualise water flux from the surface to the ceiling of Golgotha Cave. This includes annual recharge to 40 m depth in less than one hydrological year, preferential flow paths to a persistent store of water, and a time lag between soil moisture saturation and seasonal connection of karst stores that indicates a narrower window for seasonal recharge than indicated by soil moisture data.

1. Introduction

1.1. Background

In general, karst features are highly heterogeneous, fractured and complex geomorphic structures with varying degrees of permeability and hydrological flow pathways (Bradley et al., 2010; Carrière et al., 2013; Chalikakis et al., 2011). Determining the subsurface hydrology and structure of karst is often difficult due to the uniqueness and complexity of each karst system (Chalikakis et al., 2011; Gautam et al., 2000). Point and diffuse infiltration and subsequent Ca-solution leads to the formation of karst that can contain three categories of porosity such as solid to porous rocks, joints and fractures and fluid conduits (Carrière et al., 2013; Ford & Williams, 2007).

The climate-sensitive chemical signatures captured in individual stalagmites are particularly sensitive to the high level of variability in soil and rock characteristics, hydrological flow pathways, infiltration trajectory and cave morphology in an underlying karst region (Baker et al., 2015, 2000; Chalikakis et al., 2011). Thus, assessing and understanding the complex karst morphology as well as the associated hydrological flow patterns are essential for the interpretation of climate-related chemical signals stored in stalagmites.

Different methods are used to understand water movement in karst systems. Tracer experiments are frequently and successfully applied in various studies around the world (Benischke et al., 2007; Goldscheider, 2015; Goldscheider et al., 2008). They provide a reliable way in understanding transit time and pathways of water from source to sampling point. Chemically stable and radioisotope tracers are commonly employed to track subsurface water movement. These have the advantage of having a chemically distinct and unambiguous signal but require

* Corresponding author.
E-mail address: matthias.leopold@uwa.edu.au (M. Leopold).

https://doi.org/10.1016/j.jhydrol.2020.125810

Available online 1 December 2020

continuous follow-up with high resolution monitoring and prior knowledge of the site in order to determine where to introduce the tracer to minimise potential dilution, dispersion and chemical adsorption. Additionally, tracers work best when soil is removed on the surface and the fluids are directly injected into the karst system (Goldscheider 2015) which is difficult to employ in ecologically sensitive areas, especially in National Parks.

Dating dripwaters is another possibility to gain understanding of karst hydrology and flow paths. Usually, radiometric isotopes are used for dating water. However, tritium for example is often too low in concentration and precise age estimates require measurement of the daughter isotope ^{3}He which provides a challenge in cave environments owing to the potential for re-equilibration between drip and cave air (Yamada et al., 2008). Furthermore, radiocarbon (^{14}C) age measurements of water are challenging in limestone karst systems owing to dilution of the $^{14}C/^{12}C$ ratio by radioactively dead C from the limestone (Fohlmeister et al., 2011). These methods also provide information on the transit time only and not necessarily the bigger hydrological picture overlaying the cave systems i.e., trajectory of water movement, zones of water storage and hydrological connectivity throughout the system.

Subsurface geophysics, in particular 2D time-lapse electrical resistivity tomography (TL-ERT), is considered a suitable method to investigate key hydrological and geological features from the wide application in contemporary karst studies (Campbell et al., 2017; Cardarelli et al., 2006; Carrière et al., 2013; Valois et al., 2010; Watlet et al., 2018). ERT is a minimum-invasive, advanced geophysical method used to measure the electrical resistivity of the targeted soil/rock volume (Brunet et al., 2010; Loke, 2014; Samouëlian et al., 2005). Spatial and temporal variations in the electrical resistivity of subsurface matter can be utilised to distinguish the subsurface heterogeneities, such as changes in sediment mineralogy and texture, lithology, water content, temperature and salinity (Binley et al., 1995; Leopold et al., 2013; Park et al., 2014). In the context of cavity studies, variations in the electrical resistivity over time are often considered dependent to fluctuations in the water content due to the long-term stability of the subsurface. The strong contrast of resistivity values between water stores and air-filled caves ensures ERT is a suitable technique to map karst subsurface features (Carrière et al., 2013; Daily et al., 1992; Keshavarzi et al., 2017; Robert et al., 2011; Zhou et al., 2002). Studies have combined other geophysical methods such as ground penetrating radar (GPR) or electromagnetics (EM). However, GPR surveys in karst environments are often limited in exploration depth because residual clays attenuate the electromagnetic signal close to the surface (Anchuela et al., 2009). Additionally, karst environments often include bare, rough rock surfaces which contribute to poor contact with GPR antennae leading to subsequent post processing challenges.

2D ERT has been successfully used to monitor the variability of electrical resistivity to image subsurface hydrological features over time (Al Hagrey, 2007; Binley et al., 1995; Brunet et al., 2010; Samouëlian et al., 2005; Vanderborght et al., 2005; Watlet et al., 2018). Changes of electrical resistivity over time can be also used as a tool to infer flow trajectory and water storage mixing (Pakzad et al., 2008). For example, Al Hagrey et al. (1999) were able to document the large-scale distribution and movement of infiltrating rainfall throughout the subsurface using time-lapse ERT. Similarly, previous studies have tracked the migration of water in the subsurface from irrigation (Barker & Moore, 1998; Michot et al., 2003). Although 2D ERT successfully detects the movement of large-scale infiltration and flow, there are few studies that aim to detect small-scale flow pathways such as fractures and preferential flow pathways (Al Hagrey et al., 1999; Chalikakis et al., 2011). Studies have also applied ERT to delineate soil horizon and subsurface lithology from variations in electrical resistivity values (Michot et al., 2003; Zenone et al., 2008). Variations in the subsurface soil horizons and bedrock lithology are detected from the changes in electrical resistivity values due to the different permeability and water content of each material. Resistivity values tend to increase in karst features with a dense, dry rock, while they tend to decrease in regions with a more porous, moist and partly saturated limestone (Chalikakis et al., 2011).

1.2. Objectives

This study applies 2D ERT to investigate and monitor the subsurface hydrological and geological characteristics above a limestone cave in Western Australia. 2D ERT was conducted in a time-lapse mode and combined with additional soil-sedimentological and hydrological tests to understand the bigger picture of water flux from the surface to the ceiling of Golgotha Cave.

Thus, the objective of this study was to visualise water storage, wetting fronts and potential preferential flow paths and document seasonal as well as year to year changes. Furthermore, the TL-ERT was set to document the transit time and potential lag time to areas of the cave which are currently actively dripping vs dry ceiling areas.

Results will help to conceptualise a model of the flow pathways derived from ERT surveys and cave water monitoring results.

2. Material and methods

Golgotha Cave (34°05′S, 115°03′E; Fig. 1), located 20 km south from Margaret River in Western Australia, was formed in the Spearwood System (Hall & Marnham 2002) of the coastal dune aeolianite that was formed during the Late Quaternary (Lipar & Webb, 2014; Tapsell et al., 2003; Grimes, 2006). The dune limestone contains a high matrix porosity that supports primary permeability in the karst layers (Bastian, 1996; Lipar & Webb, 2014; Grimes, 2006; Vacher & Mylroie, 2002). Karstification of this limestone is occurring syngenetically with the cementation of the limestone itself (Jennings, 1968). Augering of the shallow sands above the limestone at the cave site indicate an unconsolidated surface cover between 0.3 to at least 3 m thick (the maximum length of the auger; Treble et al., 2013) consisting predominantly of fine to coarse sand-sized particles with a high permeability.

Solution pipes of variable diameters and depths are a common phenomenon in the aeolianites of Western Australia in general and they are specifically documented in the nearby Giants Cave and Caldardup Cave at up to 40 m depth. These pipes may act as vertical pathways with extremely high hydrological conductivity potentially concentrating water flow to deeper parts of the karst (Fig. 2).

This study site is located in a Mediterranean-type climate, which is associated with wet and cool winters and dry and warm summers. The nearest Bureau of Meteorology station is at Forest Grove (station ID 9547), approximately five km northeast of Golgotha Cave, for which the 30 year climatological mean annual rainfall amount is 1136 mm of rainfall, although 77% of annual rainfall is experienced in the cooler months between May and September (Bureau of Meteorology 2020). Modelled climate parameters for the cave location from the Australian Water Availability Project (AWAP) and the Australian Water Resource Assessment-Landscape model (AWRA-L) datasets (Raupach et al., 2011; Viney and Vaze, 2015) are precipitation 1106 mm and precipitation minus actual evapotranspiration 877 mm calculated for the period 1961–1990. Golgotha Cave is located in the Boranup Forest which is a mixed wet eucalypt forest of karri and marri (*Eucalyptus diversicolor and Corymbia calophylla, syn. Eucalyptus calophylla*) of 20–40 m canopy height. Tree roots are visible in the ceiling of Golgotha Cave at one location that is approximately 40 m deep. Golgotha Cave lies above the regional groundwater table which can be expressed as standing water in caves at lower elevation in the region.

The forest surface above Golgotha Cave forms part of a south-facing hillslope that intercepts rain-bearing frontal systems from the southwest. Thick organic soil layers together with highly permeable sandy soils facilitate efficient drainage supported by observations of little surface runoff despite the up to 20% land surface slope at some parts. Soil water tension time series have been collected for this soil at multiple depths to 3 m at daily interval (with some data gaps) from 2006, with data from 2006 to 2012 presented in Treble et al. (2013). These soil

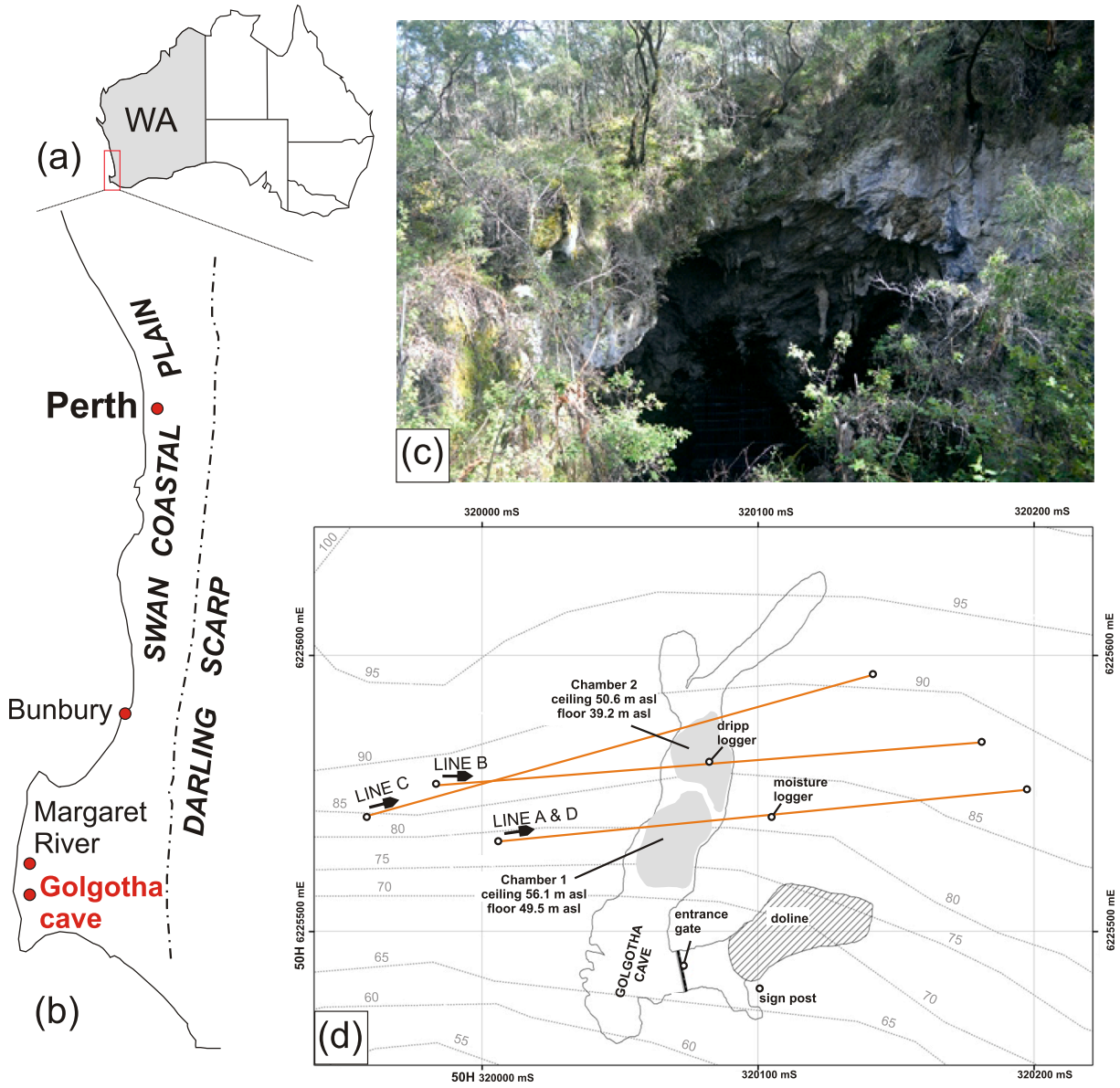

Fig. 1. Overview of the study site near Margaret River in Western Australia (1a & b). 1c, image of the entrance of Golgotha Cave in the karri forest. 1d overview of the arrangement of electric resistivity lines above Golgotha cave in relation to the two main cave chambers. Water analysis and collection of stalagmites for paleo-environmental reconstruction were conducted in Chambers 1 and 2. Note: line D (99 m) runs along parts of line A (198 m) sharing the same center point but with a smaller electrode spacing.

moisture data indicate an annual pulse of water movement through the 3 m soil profile every austral winter, with differences in timing due to antecedent climate conditions.

Golgotha Cave is accessed via a single doline-type entrance at the base of a cliff that is roughly 20 m high. The cave extends approximately 200 m into the hillside and consists of two main chambers (Fig. 1). The chambers house the longitudinal cave monitoring study that began in 2005 (Treble et al., 2013, 2015, 2016). Two arrays of automated drip loggers were also installed in 2012 in each chamber (Mahmud et al., 2016, 2018). Mahmud et al. (2018) showed that four drip types could be classified. The dominant drip discharge characteristic is a very slow continuous drip discharge, indicating the importance of matrix porosity in the thick limestone formation. Drip sites where fracture-flow was inferred generally had higher and more variable drip rates and exhibited a delayed threshold response of drip rate to the wet winter of 2013. In Chamber 1, there was a greater spatial homogeneity of drip discharge, with clusters of similarly classified drips, compared to Chamber 2. There, a greater heterogeneity of flow paths were inferred.

Morphological classification of stalactites using LiDAR-based imagery was conducted to classify flow types as either matrix, fracture or a combination of matrix, fracture and conduit flow (Mahmud et al., 2015, 2016). Using the mean drip discharge for each stalactite classification type Mahmud et al. (2016) calculated a mean water flux into the ceiling of the cave. In Chamber 1 this was 840 mm yr^{-1} per m^2 and in in Chamber 2 it was 1170 mm yr^{-1} per m^2, with a greater proportion of active stalagmites in Chamber 2 attributed to its lower relative elevation, and the influence of hydraulic gradient on water movement in this area. Water balance considerations suggest that infiltration was focussed to specific areas of the cave ceiling, and that the cave had a capillary fringe effect, with less recharge entering the cave compared to the overlying surface infiltration. The period of ERT data overlap with data collected as part of the long term cave monitoring program conducted at Golgotha Cave. These data are presented here as updated measurements coinciding with the ERT surveys.

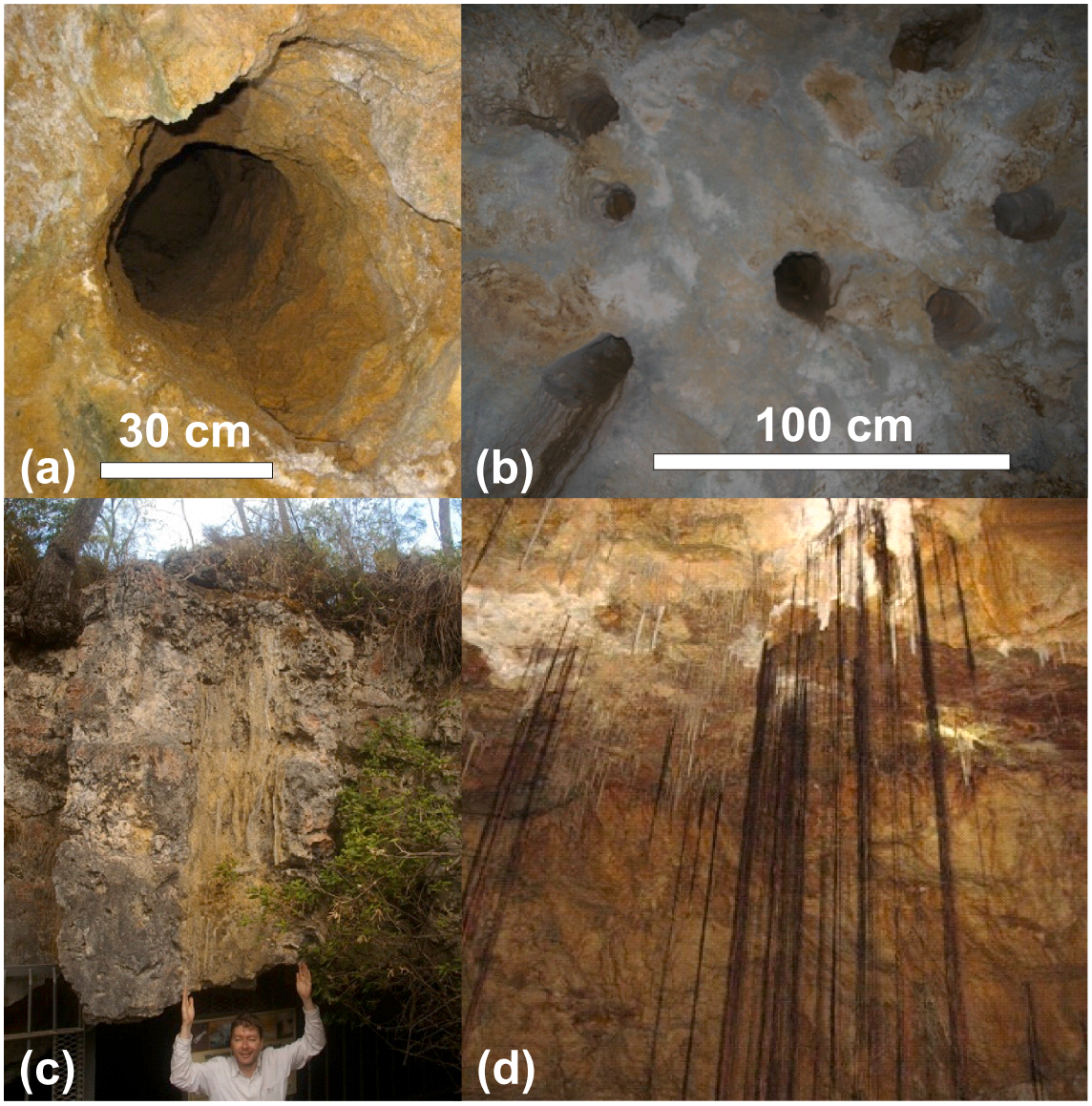

Fig. 2. Collage of vertical pipes exposed at Caldardup Cave and Giants Cave, both within a 6 km distance of Golgotha Cave. 2a) Close up of pipe with soil/sediment filling visible at upper end of pipe. 2b) An assemblage of 10 smaller pipes distributed across roughly 2 m^2. 2c) A larger pipe with approximately 80 cm diameter, person for scale. 2d) Active tree roots occupying pipe holes and hanging from the ceiling of Calgardup Cave approximately 30 m below the surface.

Multiple ERT survey lines (line A to D, compare Fig. 1) were established in order to determine both temporal and spatial information on water movement above and near the cave. Specific parameters of each line are given in Tables 1 and 2. Note, line A and D are running along the same direction, with line D providing a 100 m long high resolution (1 m electrode separation) segment of line A (2 m electrode separation). Table 3.

Time-lapse surveys (Line A/F and Line B; Table 2) were conducted

Table 1
Basic parameter of the various electric resistivity lines used in this study.

Name	Length	Spacing	Numbers of electrodes	Array type	Array type
	[m]	[m]		Wenner	Dipol-Dipol
LINE A	198	2	100	x	x
LINE B	198	2	100	x	x
LINE C	198	2	100	x	x
LINE D	99	1	100	x	x

Table 2
Overview of survey dates, seasons, times and temperatures as part of the time-lapse approach of this study.

YEAR	DATE	SEASON	surface temp °C/at time	LINE A	LINE B	LINE C	LINE D
2016	16-May	Autumn	12.3 °C/ 12:00				x
2016	2-Aug	Winter	11.3 °C/ 15:00	x			x
2016	3-Nov	Spring	11.0 °C/ 09:00	x			x
2017	4-Feb	Summer	15.4 °C/ 08:00	x			x
2017	5-Aug	Winter	12.8 °C/ 15:00	x			x
2017	6-Oct	Spring	12.3 °C/ 11:00	x	x	x	
2018	12-Jan	Summer	14.6 °C/ 07:00		x		

Table 3
Basic physical parameters of a soil and two rock types representing the variability of material in this study.

sample no.	position	material	bulk density [g cm^{-3}]	porosity
1	surface layer	sandy soil	1.65	0.38
1	entrance cliff	calcarenite fragment	1.89	0.30
2	entrance cliff	calcarenite fragment	2.36	0.13

over the long-term monitoring locations above the cave Chambers 1 and 2, respectively. Chamber 1 is the principle location that speleothem records are being developed for paleoclimate reconstruction. Line A and F also intersect the location of long-term monitoring of soil moisture data (Treble et al., 2013).

The DC-electric resistivity meter 4-point light hp from Lippmann Geophysical Instruments (Lippmann, 2008) was used in combination with 100 active electrodes. Electrodes consisted of 8 mm thick and 30 cm long stainless steel poles which remained in the ground for the time-lapse survey during the study. Winter and spring surveys were conducted during sunny days in early afternoon and summer and autumn surveys took place during overcast days with cloud cover in the mornings in order to compensate surface temperature differences during the seasons as much as possible. Each measurement point of the combined Wenner and Dipole-Dipole arrays was repeated three times and values were recorded if they showed a difference below 1% resulting in 2779 data points for a 100 electrode section. In case higher differences were observed, points were repeated at least five times and subsequently averaged. Measurement points above 5% difference were subsequently deleted with less than 0.2% of all points removed. Geotest 2.50 (Geotest 2019) was used as acquisition software which also automatically regulated the conducted current usually between 1 mA and 50 mA with a measurement frequency of 4.16 Hz. Resulting apparent resistivity values were exported to RES2DINV from Geotomo software (Loke, 2014) where individual pseudo sections were inverted using a least mean square approach. Usually 4–7 iterations were conducted until the convergence limit of 2% was reached. Iterations initially started with a damping factor of 0.15 and finally with a minimum of 0.03 resulting in absolute differences of 2–8% between measured and calculated apparent resistivity values. For time-lapse analysis specific electric resistivity values were exported to MS Excel for further calculations. We used values of the driest condition as a reference to display changes between time series using equation (1).

$$\Delta p = \left(\frac{logpo}{logpi}\right) * 100 \quad (1)$$

p_0 = highest observed resistivity value for each model cell; pi = resistivity value of comparing time step

Displaying results using the logarithm of resistivity values provides better visualisation of gradual spatial variation as suggested by Watlet et al. (2018). Negative values indicate that the area experienced a decrease of resistivity between time steps which is consistent with increase of moisture during different seasons and vice versa.

Additionally, two rocks (aeolianite, ~ 10 × 10 × 8 cm) with different porosities from the cave's entrance cliff and a sample from the sandy surface soil were collected and tested for their electric resistivities in the laboratory under controlled temperature conditions (15 °C). Stainless steel nails with a spacing of 1.5 cm were mounted on rock samples in 0.5 cm deep drill holes and used as electrodes to measure resistivity using a wenner array. Sediments and rocks were saturated with deionised water for 24 h and placed on a laboratory scale to measure weight loss due to evaporation over time. Electric resistivity values and weight loss were recorded hourly until weight losses neared zero. Volumetric moisture contents (θ cm^3/cm^3) vs electric resistivity values were plotted for the three different rock/soil types and fitted to a power law trendline. Since our intention was a relative comparison, we avoided fitting the data to a petrophysical model such as Archie's law (Archie, 1942) by assuming 1/Ro is uniform and displayed a simple power law relationship.

3. Results

A sandy soil and two rock samples collected at the study site showed a strong power law correlation between volumetric water content (θ) and electric resistivity (Ωm) with R^2 values > 0.9 (compare Fig. 3). This is important information as it strengthens the interpretation of the time-lapse study in a way that observed changes in resistivity will be caused by different volumetric water contents. Other factors influencing resistivity such as temperature were neglected for our study, because thick vegetation and loose topsoil buffer heat fluxes and the variability of near surface temperatures was limited during the individual surveys (compare Table 2). Treble et al. (2015) also document a very stable cave temperature throughout the year further supporting the validity of this assumption. Additionally, the electric conductivity of the water is assumed to be very constant during the year as drip water collection shows a low standard deviation for certain elements especially Na which is linked to potential salt input via rainfall throughout the year (Treble et al., 2016). Differences in the materials and their porosities lead to different volumetric water contents for similar electric resistivity values. In this case, attempts to directly translate resistivity changes into water

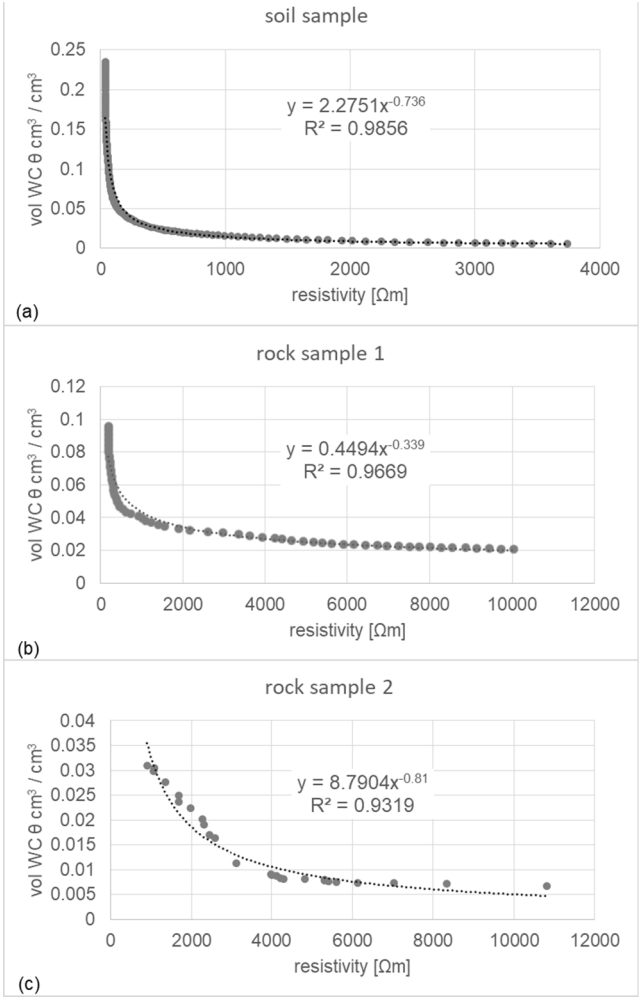

Fig. 3. Power law correlations between volumetric water content (θ) and electric resistivity of a sandy surface soil (a) and two different rocks (b, c) from the study site. Note differences in x- and y-axle values between samples.

contents are difficult without precise geologic and stratigraphic knowledge of the survey line which we don't have at our site. However, additional rock samples from the cave ceilings showed similar porosities of > 0.3. Thus, results of Fig. 3 are an important interpretation guide, as we can expect sandy soils and porous rocks, or zones with abundant cracks and pipe conduits will provide a large range of electric resistivity values over a season compared to dense rocks with a low porosity. Zones with constant resistivity values above 3000 Ωm only experience a maximum of 1% change in volumetric water content over the year. Soils and porous rocks can be expected to display anything from ~200 to 3000 Ωm depending on the season and thus volumetric water contents (θ) between 0.02 and 0.25 cm^3/cm^3 (compare Fig. 3). Overall the following ERT-hydrogeological zones were identified:

Z1, is a zone where large differences in electric resistivity were observed, from as low as 100 Ωm during the winter to more than 5000 Ωm during the summer across the whole range of resistivity values identified in Fig. 3a-c. These values reflect the wetting and drying of near surface soils and porous rocks in accordance with the annual change in precipitation and temperature. Values are in accordance with similar sandy soils from Western Australia (compare Lowe et al., 2017).

Z2, is a zone that reflects low resistivity values of less than 800 Ωm and it is located below Z1. The low values are more constant during the

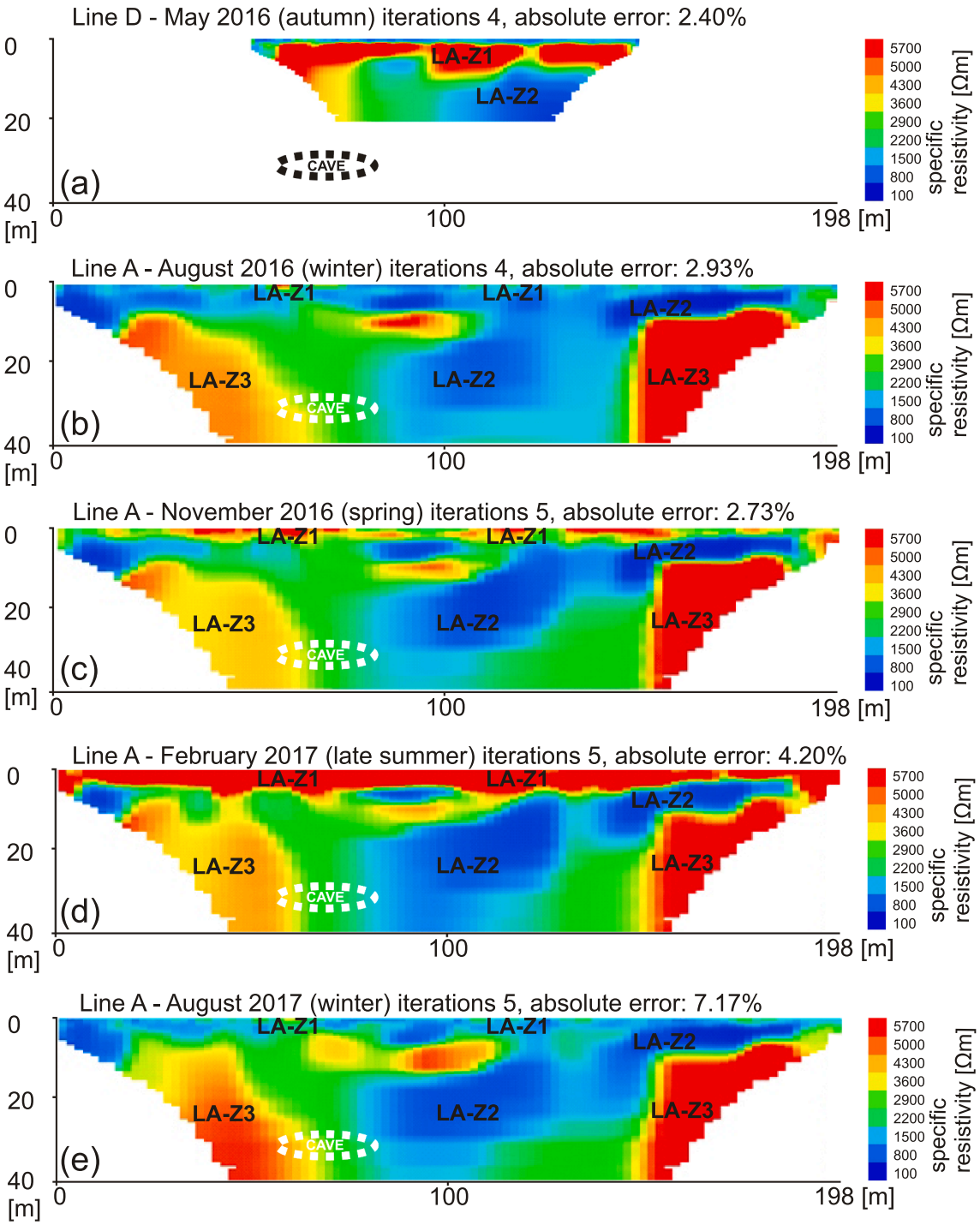

Fig. 4. The specific electrical resistivity distribution of line A above Golgotha Cave over the season 2016 to 2017. Note, line D in 3a is along the same survey line as line A but reveals a higher resolution yet shallower depth of exploration. LA-Z1 to 3 indicate ERT-hydrogeological zones of line A.

year and thus less connected to the timing of annual rainfall. They reflect the steeper parts of the curves in Fig. 3a, b. However the resistivity values tend to decrease slightly during the summer indicating a lag time between infiltration and percolation of the winter rain at deeper parts of the survey lines.

Z3, is a zone where electric resistivity values were above 3000 Ωm throughout the year. It reflects the flat parts of the curve in Fig. 3c and is interpreted as solid rock which allows limited water infiltration and percolation.

Fig. 4 displays the specific electric resistivity sections for different seasons between 2016 and 2017 for line A, which runs from west to east for 198 m. Values ranged from 100 to 6000 Ωm reflecting different materials and moisture regimes of the vadose zone (compare Fig. 2). The ceiling of Chamber 1 is located near the middle of the line at ~ 30 m depth (compare Mahmud et al., 2016). However, no change of resistivity is registered at this depth and location. Putiška et al. (2012) described similar difficulties in detecting caves using ERT and linked it to highly conductive thin layers caused by moisture and clay accumulation around the caves. In Golgotha Cave a palaeosol, enriched in clay minerals and moisture is visible at the ceiling of Chamber 1 (Treble et al., 2016) which might cause a deformation of the equipotential lines and force the current flow around the cavity preventing the cave to appear in the ERT sections.

Mahmud et al. (2016) calculated a water balance which indicates that about 20% of the water may be flowing around the cave with the cave ceiling acting as a capillary barrier providing a further explanation why the cave is not detected in the ERT sections. Additionally, by using ERT the overall model sensitivity decreases with depth.

The western and eastern sides of the survey in Fig. 4 each display a zone of high resistivity (LA-Z3 in Fig. 4) starting at 6 to 8 m depth and extending through the surveyed depth for which the resistivity values are consistent throughout the year. We interpret this zone as a more cemented rock below the soil zone similar to the description by Lipar & Webb (2015). In contrast, the upper 0 to 6 m as well as the central parts of the sections substantially change in electric resistivity over the year between 100 and 5000 Ωm (LA-Z1 in Fig. 4).

In general, the LA-Z1 showed low resistivity values during winter but increased towards summer which is consistent with earlier soil moisture time series (Treble et al., 2013). From roughly 15 m depth in the central parts and 10 m depth in the eastern parts we observe resistivity values between 100 and 800 Ωm (LA-Z2 in Fig. 4). LA-Z2 is interpreted as a persistent store of water rather than a zone with higher clay contents, since clay in the Tamala limestone is associated with palaeosols that are restricted to ~ 1 m thickness (Lipar & Webb, 2014). However, it is possible that either a palaeosol or older caprock layer is assisting the perched appearance of this feature. The spatial extent and resistivity values of LA-Z2 also varies intra- and inter-annually, further supporting that this zone is depicting water storage. Hence LA-Z2 is interpreted as aeolianite with relatively higher porosity and permeability which function as water storage and flow pathways throughout the year. During the summer these low resistivity sections decrease in their electric resistivity value with greater depth indicating fluids moving through the vadose zone towards the cave to deeper sections at that time of the year.

In the centre of the line close to the cave LA-Z2 extends to the depth of the cave ceiling. This indicates permanent moist conditions particularly on the eastern side of the cave. Resistivity is relatively lower deeper in the profile beneath this store in February 2017 indicating increased water movement to lower depths approximately 6 months following infiltration. This store of water becomes connected to seasonally infiltrating water, evident during the winter in the August 2016 and August 2017 surveys. This connection appears to be via a localised area of inflow from the surface around 120 m along the line. It also appears to be connected to the shallow low resistivity section interpreted as water store on the eastern edge of the line which overlies an area of permanently high resistivity.

Lines B and C are two additional 198 m long ERT lines north of line A (Fig. 5). These additional lines were set up to determine the extent of the identified water storage (LA-Z2) in line A and to further discuss if the observed water movement is mainly vertical and interflow downhill can be excluded.

Line B runs approximately 25 m north of line A directly above Chamber 2 of the cave, which again could not be identified in the image. Similar to line A the 2D-tomography allows the identification of three distinct zones separated by their specific resistivity values. LB-Z3 is characterised by values larger than 3500 Ωm during spring and summer and is interpreted as solid rocks that restrict water infiltration. LB-Z1, which expands across the whole line down to about 6–8 m, represents the zone of annual saturation during the winter and drying during the summer. LB-Z2 represent areas that are permanently wet regardless of the season. They are connected to the surface infiltration during the winter months and act as water storages for the cave. However, similar to Line A, the location of LB-Z2 is further to the east of the cave and appears to be hydrologically connected to the eastern but not the western part of the cave.

Line C crosses the cave at the very northern end of Chamber 2 and was set up to identify potential interflow along the hill into the permanently saturated zone of LB-Z2. The central part of the survey line is characterised by higher resistivity values (LC-Z3) characteristically for more solid rocks. The low resistivity zone Z2, which was identified in line A and B, is only vaguely present to the east of the cave but an additional more prominent Z2 was identified at a deeper level to the west in line C. The latter is likely to be located too far to the west of the cave to be hydrologically connected to Chamber 2.

Comparing lines A-C, a common feature is a hydrologically connected and persistent water store to the eastern side of the cave (Z2).

During August 2016 the homogenous infiltration down to 6–8 m is visible (Fig. 6). Central parts as well as areas to the west and mainly east have their driest condition during this time because the new rain has not yet percolated to these depths. During November 2016 the near surface infiltration zone is less pronounced and spatially more heterogeneous with drier conditions on the surface. In general deeper parts of the surveyed line show largely negative values with a very prominent near vertical area at around 160 m. This zone is directly besides the area that was further above identified as near solid dry limestone. It could be an important large preferential flow path into deeper parts of the karst. In February 2017 near surface Δ-log resistivity values tend to zero indicating that hardly any moisture remains at 6 m depth (Fig. 6). Deeper down the profile small negative values indicate that most areas receive additional water, this includes the rather dry parts of the west and east side interpreted as solid rocks with only small cracks. However most noteworthy is that Z2 areas that are already moist throughout the year receive additional moisture during summer when the water that infiltrated during the previous winter finally arrives at 40 m depth. This pattern is largely repeated again in Aug 2017 when the near surface wets up again and large areas further down remain moist with some additional water gain. In general a continuous supply of water to the cave ceiling is documented and the survey confirms a lag of approximately up to 12 months after infiltration for the water to reach the cave ceiling. However on the eastern side it looks as if preferential flow is established where water might be perched by the rather dense rock and directed towards the preferential flow area located at 160 m where it then infiltrates quickly into deeper parts of the karst to the east of the cave.

Trees such as the karri, endemic to the south west of Western Australia, are known for their ability to create or aid the development of pipes in limestones (Grimes 2006). Active, living roots of these trees were observed in Golgotha Cave and in other caves in the region at depths of up to 40 m. Our measurement lines located several features throughout different times of the year where we expect vertical preferential flow paths most likely caused by sub-surface pipes (Fig. 7). Depiction of such features was between 0 and 5 m depth where the resolution of the ERT section is highest but they could not be detected at

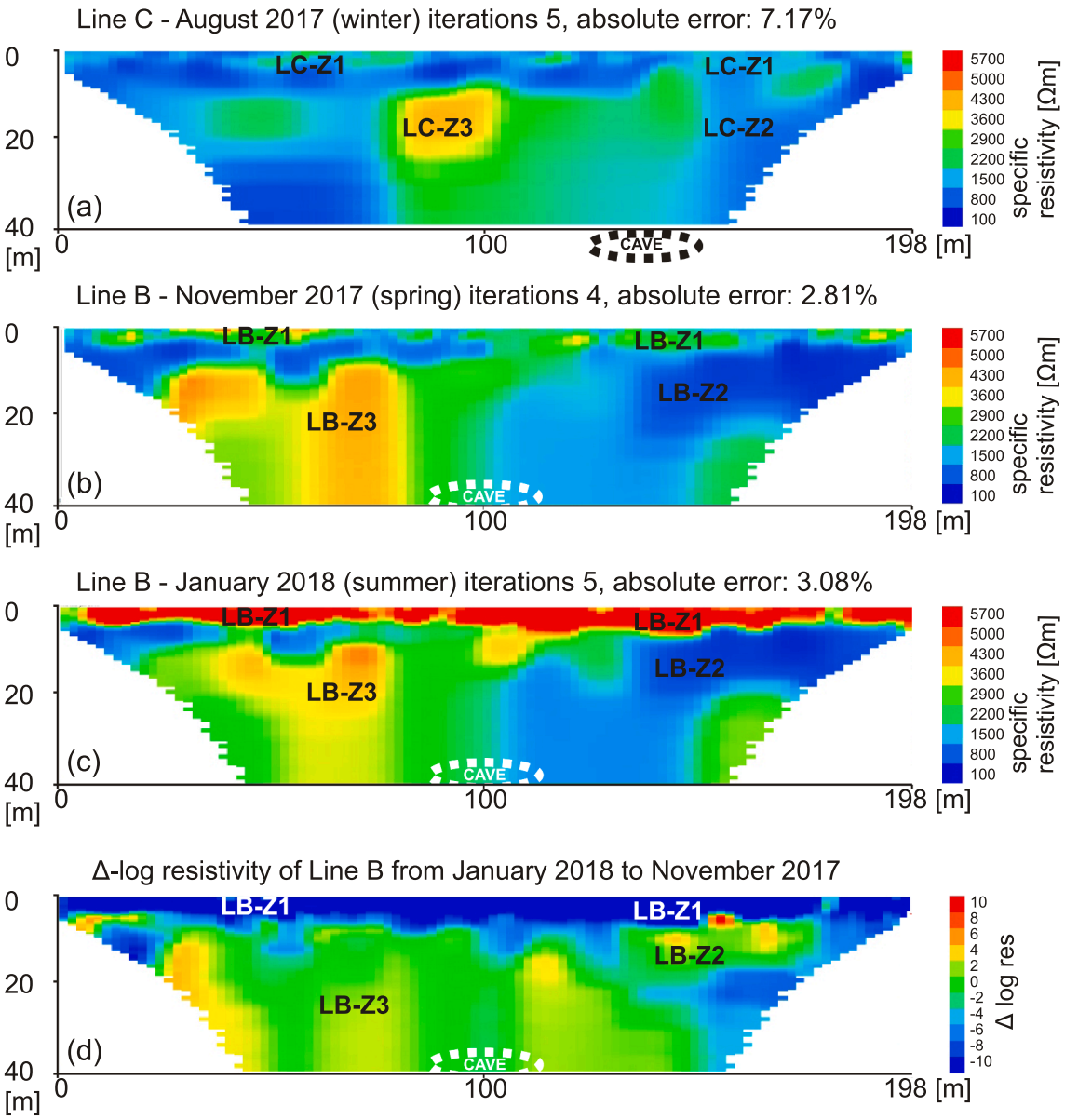

Fig. 5. The specific electrical resistivity distribution of line B and C above Golgotha Cave during different seasons (5a-c). The exploration depth of Line C did not reach the cave ceiling. 5d displays the Δ-log resistivity distribution between summer and spring along line B. LB-Z1 to 3 indicate ERT-hydrogeological zones of line B and LC-Z1 to 3 of line C respectively.

greater depth. In general, features associated with pipes are located more towards the east of the cave, probably providing a fast hydrologic pathway to the more persistent subsurface water storage in this area as introduced above (LA-Z2 and LB-Z2). It must be noted that these features may be a combination of pipes and doline formations since some of the features seen in Fig. 6 are up to 2 m wide.

4. Discussion

The time-lapse ERT survey reveals changes of electric resistivity values that can be linked to seasonal water movement consisting of a wetting front. During each wet winter season it develops to a depth of up to 10 m (ERT-hydrogeological zone Z1 in lines A-D). During the following dry summer Z1 mostly dries up reflecting a Mediterranean type climate typical for the area (Charles et al., 2010). Vegetation with shallow roots does not have access to year round moisture especially in the upper 1–2 m and often dies or goes dormant during the summer.

Parts of the annual recharge percolate to deeper depths during the months following winter and the TL-ERT surveys indicate downward water movement to the depth of the cave ceiling in less than one hydrological year. We observed a reduction in resistivity values starting in November 2016 and continuing to February 2017 between 20 and 40 m depth in selected, spatially variable areas (ERT-hydrogeological zone Z2). This resistivity reduction likely displays percolation of water in deeper karst stores. Mahmud et al. (2016) observed a threshold response in drip rates from stalactites dominated by hydrological fracture pathways with a lag of 3–6 months after infiltration which is consistent with our observations of piston flow response to the percolation of water to deeper stores.

The water movement in deeper sections near the cave (~40 m) can continue during the following dry season but is decoupled from the surface infiltration as indicated during August 2017 (Fig. 6c, ERT-hydrogeological zone Z2 near cave). Our automated drip loggers indicate that the net percolation at depth via fracture pathways depends on the amount of rainfall during the previous season (Mahmud et al., 2016; see also Fig. 8). This is corroborated here in our TL-ERT study. In the two

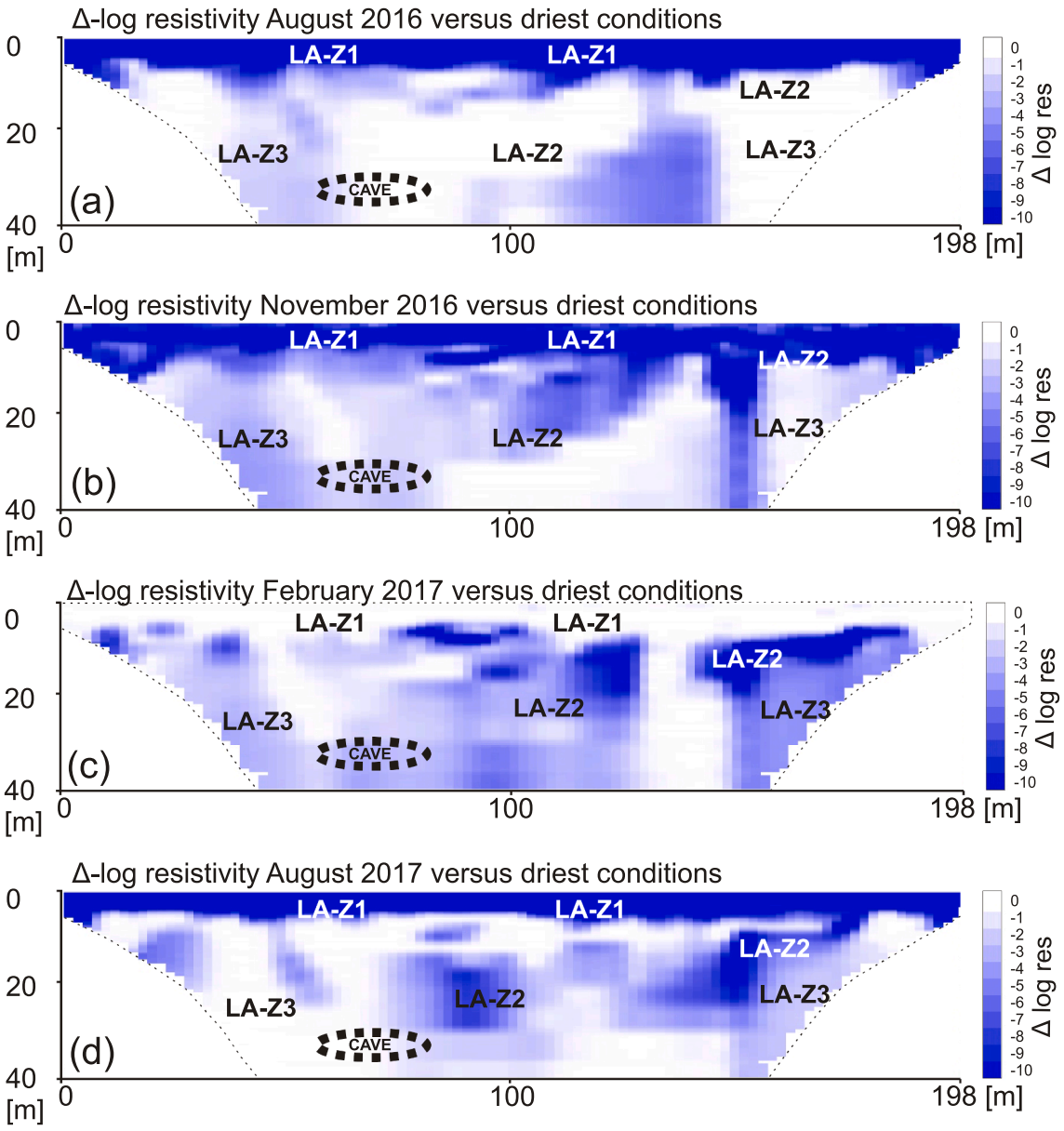

Fig. 6. Images of individual time steps (a-d) compared to the driest condition (highest resistivity value) measured during the whole campaign along line A. Thus, values around 0 (white) indicate areas under driest conditions, whereas negative (blue) values indicate where, how much and at which time of the year we observed changes due to additional water infiltration. LA-Z1 to 3 indicate ERT-hydrogeological zones of line A. (For interpretation of the references to colour in this figure legend, the reader is referred to the web version of this article.)

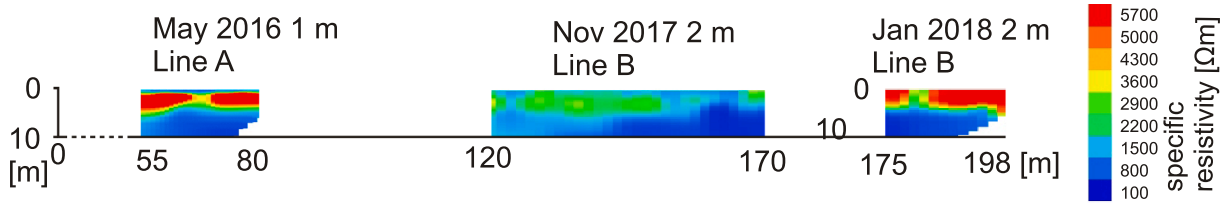

Fig. 7. Examples of sections of various electric resistivity lines reproduced at higher spatial resolution displaying pronounced horizontal interruptions of the near surface layer. Grey arrows indicate these locations which are interpreted as preferential flow paths probably linked to solution pipes.

years preceeding our ERT survey (2014 and 2015) total annual rainfall for the cave site was relatively low (982 mm and 829 mm respectively; 2015 was below the 5th percentile of the climatological mean). Drip rates from our drip loggers indicate that stored water feeding the cave system was declining during these dry years (Fig. 8). Our ERT surveys began in 2016, a relatively wet year (1148 mm) during which drip rates responded to this higher rainfall, increasing from about November 2016, indicating enhanced recharge of karst stores in response to the 2016 wet season (Fig. 8). This is evident in the ERT images (Figs. 4 and 6). In August 2016, the infiltration from this relatively wet winter season is

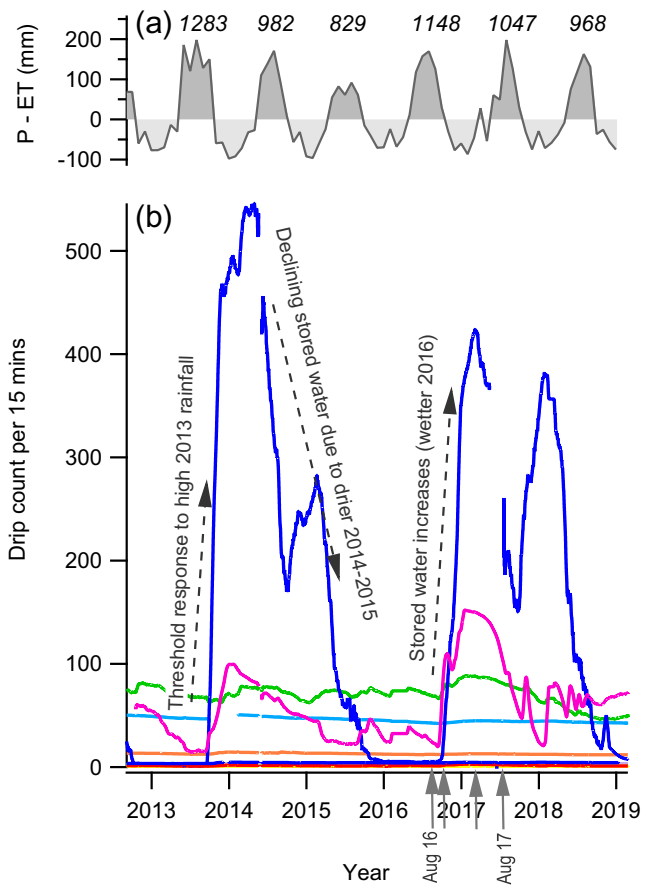

Fig. 8. Monthly precipitation minus evapotranspiration (a), and selected drip rate time series measured in the automated drip logger network described in Mahmud et al. (2016) (b). Adapted from Mahmud et al. (2016) and updated to include the period of TL-ERT measurements. Arrows on x-axis indicate timing of ERT surveys. Italicised numbers are annual rainfall totals at Golgotha Cave. High drip rates with high response to infiltration are connected to fractures while low, smoothly varying drip rates are dominated by matrix flow.

still in the shallow zone (LA-Z1; Fig. 6a); the subsequent percolation of this water is seen in Fig. 6b-d. Comparing Fig. 6d with 6a shows that infiltration from the 2016 wet season has resulted in greater recharge (saturation and spatial extent of saturation) in zone LA-Z2 and below this zone (Fig. 6d) compared with the previous hydrological year (Fig. 6a).

The difference in drip rates associated with either fracture or conduit flow for fast dripping sites versus flow through the matrix for slow dripping sites was already described by Mahmud et al. (2015, 2016). The spatial resolution of ERT effectively displays both percolation types at a coarser resolution, with slow matrix flow in soils and porous rocks and areas of focussed recharge that likely relate to water movement into, and leakage from, tubes and solutionally widened fractures.

ERT was also able to display several large vertical features that most likely represent pipes described by Grimes (2006). However the features displayed in Figs. 6 and 7 are between 1 and 2 m wide. Tests using resistivity modelling software RES2DMOD showed features with diameters smaller than 1 m (Fig. 2) or cracks are below the horizontal resolution limit of the applied arrays and electrode spacing (Loke, 2014). Although features smaller than 1 m are known from other caves in the vicinity, we assume that a cluster of smaller tubes as shown in Fig. 2b will lead to a zone with reduced specific electric resistivity values when filled with wet sediments.

Time-lapse ERT at different locations shows there is a persistent store of water that is hydrologically connected to the eastern margin of the cave (ERT-hydrogeological zone 2 in line A-C). It is supplying the eastern flanks of Chambers 1 and 2 with greater water movement compared to the relatively drier areas of the western side of the cave. This 'divided moisture regime' with greater water flux and storage along the eastern flank of the cave is consistent with the general increase in drip rates towards the eastern wall (Mahmud et al., 2016; 2018) and our field observations of the density of cave calcite decorations as an indicator of flow paths (Fig. 9).

This large store is likely to consist of numerous interconnected stores, fracture networks and zones of high porosity and permeability. This is supported by our drip logger data that indicate individual flow paths, indicated by different drip discharge characteristics such as base flow, peak discharge and response to recharge, in this area of the cave (Fig. 8; Mahmud et al., 2016, 2018). Heterogeneity between drip data increases towards the stored water mapped in this study, in contrast to greater spatial homogeneity in drip data elsewhere in the cave that are dominated by matrix flow (Mahmud et al., 2018). Comparing the proximity of this zone to the cave in lines A to C suggests that this large store of water is closer to the cave wall in Chamber 2 (lines B, C; Fig. 5) vs Chamber 1 (line A; Fig. 4). This is also supported by the more extensive calcite decoration on the eastern wall, and the typically higher drip rates, of Chamber 2 versus Chamber 1.

Soil moisture data from 0.1 to 3 m depth were presented previously in Treble et al. (2013). Fig. 10 shows that the soil is saturated to a depth of 3 m each May (±1 month) which is in agreement with our ERT data (Fig. 4a). However, the deeper profile viewed in the TL-ERT data indicate that ERT-hydrogeological zone 2 does not connect to surface infiltration until several months after. This suggests that the stored water is connected to surface infiltration for a shorter period than that suggested by the soil moisture data time series. This is consistent with field and modelling studies that have demonstrated that the epikarst can be considered as a temporary water store (Williams 1983) that stores water for up to several months (Aquilina et al., 2006; Hartmann et al., 2013), resulting in a lag between soil moisture saturation and peak recharge. Thus we suggest here that the autumn and early winter rain saturates the soil zone/upper epikarst, permitting rain later in winter to contribute most (volumetrically) to recharge into the cave via preferential flow paths. This has been simulated in lumped parameter modelling of cave drip water recharge in the European Mediterranean karst, with a modelled winter recharge bias explaining observed cave drip water $\delta^{18}O$ values (Baker et al., 2019).

5. Conclusions

Hydro-chemical data derived via drip water collection and stalagmite analyses, provide a powerful tool for cave monitoring and climate reconstruction. However, it is increasingly recognised from these data that the heterogeneity of karst hydrological systems can lead to spatial heterogeneity of hydro-chemical data, down to the scale of an individual percolating drip water site. Mixing of water through the interconnected karst voids is typically hard to constrain in cave studies and lateral input though interflow parallel to the surface can significantly blur signals from individual drip points in a cave. Knowledge about infiltration pathways and percolation times are therefore extremely important to understand the karst hydrology of infiltration waters to a cave system, and evaluate the spatial heterogeneity of water movement and improve the interpretative power of potential climate and hydrological proxies such as $\delta^{18}O$ and Sr/Ca and Mg/Ca elemental ratios.

At Golgotha Cave, TL-ERT identified an annual wetting front in combination with several vertical preferential flow pathways via pipes. In combination with the highly porous surface sand and the low slope angle makes lateral water movement via interflow unlikely. TL-ERT data displaying variations in flow regime embellishes long-term monitoring data for the cave, which identified heterogeneities in water movement at the scale of cave chambers as well as individual drips, but not the processes for this variability, and improves confidence in our understanding

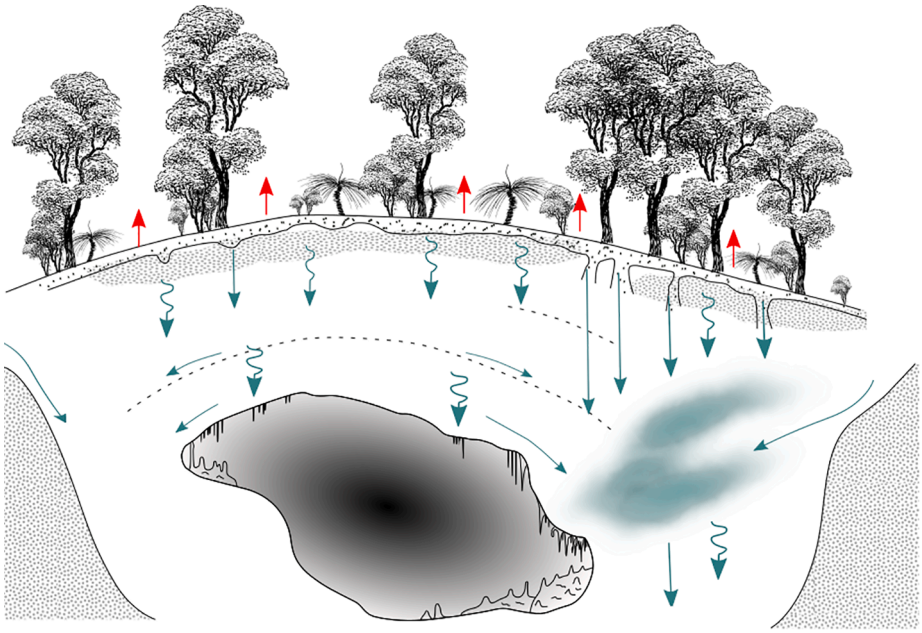

Fig. 9. Conceptual model of Golgotha Cave cross section. Cave calcite decoration (stalactites, stalagmites and flowstones) increase in density towards the walls of the cave, particularly to the east, indicating greater water movement to this area of the cave. This is consistent with the eastern store of water that was persistently observed in the TL-ERT transects. Straight arrows represent preferential flow, wiggle arrows represent diffuse flow and red arrows represent seasonal drying of the surface layer. (For interpretation of the references to colour in this figure legend, the reader is referred to the web version of this article.)

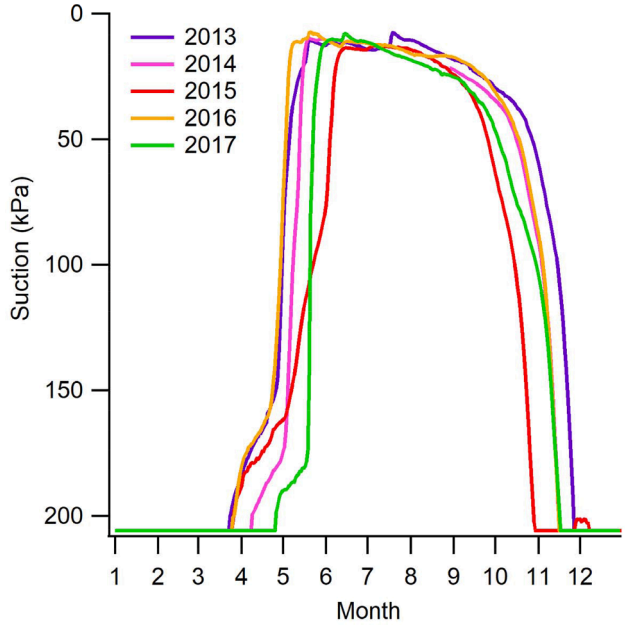

Fig. 10. Soil moisture at 3 m depth for years 2013–2017 where suction of 0 kPa represents a saturated soil.

of paleoclimate records contained within stalagmites from the cave. This is the focus of our current research. From our TL-ERT research at Golgotha Cave and long-term monitoring at the cave and elsewhere we can now propose a 'toolkit' for cave monitoring. This includes surface weather station data, automated soil hydrology monitoring networks to constrain soil moisture heterogeneity (Berthelin et al., 2020), TL-ERT profiles, automated cave drip water hydrology monitoring, within-cave LiDAR mapping of infiltration features, and cave climate and drip water chemistry monitoring.

Declaration of Competing Interest

The authors declare that they have no known competing financial interests or personal relationships that could have appeared to influence the work reported in this paper.

Acknowledgements

We thank Carolina Paice from Cape-Leeuwin N.P. for providing access and assistance in the field, Andy Spate for survey data and Alan Griffiths for precipitation and actual evapotranspiration data extracted from the AWRA-L dataset for Golgotha Cave. We further thank Mary-Anne Lowe and Larissa and Gabriel Leopold for assistance during field work. We are grateful for the comments of Sebastian Uhlemann and another anonymous reviewer as well as for the helpful comments of the editors which further improved the manuscript.

References

Al Hagrey, S.A., 2007. Geophysical imaging of root-zone, trunk, and moisture heterogeneity. J. Exp. Bot. 58 (4), 839–854. https://doi.org/10.1093/jxb/erl237.

Al Hagrey, S.A., Schubert-Klempnauer, T., Wachsmuth, D., Michaelsen, J., Meissner, R., 1999. Preferential flow: first results of a full-scale flow model. Geophys. J. Int. 138 (3), 643–654. https://doi.org/10.1046/j.1365-246x.1999.00906.x.

Anchuela, Ó.P., Casas-Sainz, A.M., Soriano, M.A., Pocoví-Juan, A., 2009. Mapping subsurface karst features with GPR: results and limitations. Environ. Geol 58, 391–399. https://doi.org/10.1007/s00254-008-1603-7.

Aquilina, L., Ladouche, B., Dörfliger, N., 2006. Water storage and transfer in the epikarst of karst systems during high flow periods. J. Hydrology 327, 472–485. https://doi.org/10.1016/j.jhydrol.2005.11.054.

Archie, G.E., 1942. The electrical resistivity log as an aid in determining some reservoir characteristics. Trans. Am. Instit. Min. Eng. 146, 54–62.

Baker, A., Hartmann, A., Duan, W., Hankin, S., Comas-Bru, L., Cuthbert, M.O., Treble, P. C., Banner, J., Genty, D., Baldini, L., Bartolomé, M., Moreno, A., and Pérez-Mejías, C., 2019. Global distribution and controls on cave drip water oxygen isotope composition. Nature Communications, 10, Article number: 2984. https://doi.org/10.13140/RG.2.2.25448.93443.

Baker, A., Hellstrom, J.C., Kelly, B.F., Mariethoz, G., Trouet, V., 2015. A composite annual-resolution stalagmite record of North Atlantic climate over the last three millennia. Sci. Rep. 5, 10307. https://doi.org/10.1038/srep10307.

Baker, A., Genty, D., Fairchild, I.J., 2000. Hydrological characterisation of stalagmite dripwaters at Grotte de Villars, Dordogne, by the analysis of inorganic species and luminescent organic matter. Hydrol. Earth Syst. Sci. 4 (3), 439–449. https://doi.org/10.5194/hess-4-439-2000.

Barker, R., Moore, J., 1998. The application of time-lapse electrical tomography in groundwater studies. Lead. Edge 17 (10), 1454–1458. https://doi.org/10.1190/1.1437878.

Bastian, L.V., 1996. Residual soil mineralogy and dune subdivision, Swan Coastal Plain, Western Australia. Aust. J. Earth Sci. 43 (1), 31–44. https://doi.org/10.1080/08120099608728233.

Benischke, R., Goldscheider, N., Smart, C.C., 2007. Tracer techniques. In: Goldscheider, N., Drew, D., (eds). Methods in karst hydrogeology. International Contribution to Hydrogeology, IAH, 26: 147-170. Taylor and Francis/Balkema, London.

Berthelin, R., Rinderer, M., Andreo, B., Baker, A., Kilian, D., Leonhardt, G., Lotz, A., Lichtenwoehrer, K., Mudarra, M., Padilla, I.Y., Pantoja Agreda, F., Rosolem, R., Vale, A., Hartmann, A., 2020. A soil moisture monitoring network to characterize karstic recharge and evapotranspiration at five representative sites across the globe. Geosci. Instrum. Method. Data Syst. 9, 11–23. https://doi.org/10.5194/gi-9-11-2020.

Binley, A., Shaw, B., Henry-Poulter, S., 1995. Flow pathways in porous media: Electrical resistance tomography and dye staining image verification. Meas. Sci. Technol. 7 (3), 384. https://doi.org/10.1088/0957-0233/7/3/020.

Bradley, C., Baker, A., Jex, C.N., Leng, M.J., 2010. Hydrological uncertainties in the modelling of cave drip-water δ 18 O and the implications for stalagmite palaeoclimate reconstructions'. Quat. Sci. Rev. 29 (17), 2201–2214. https://doi.org/10.1016/j.quascirev.2010.05.017.

Brunet, P., Clément, R., Bouvier, C., 2010. Monitoring soil water content and deficit using Electrical Resistivity Tomography (ERT)–A case study in the Cevennes area. France. Journal of Hydrology 380 (1), 146–153. https://doi.org/10.1016/j.jhydrol.2009.10.032.

Bureau of Meteorology 2020, Australian Government. Available from: <http://www.bom.gov.au/climate/data/>. [19 June 2020].

Cardarelli, E., Di Filippo, G., Tuccinardi, E., 2006. Electrical resistivity tomography to detect buried cavities in Rome: a case study. Near Surf. Geophys. 4 (6), 387–392. https://doi.org/10.3997/1873-0604.2006012.

Carrière, S.D., Chalikakis, K., Sénéchal, G., Danquigny, C., Emblanch, C., 2013. Combining electrical resistivity tomography and ground penetrating radar to study geological structuring of karst unsaturated zone. J. Appl. Geophys. 94, 31–41. https://doi.org/10.1016/j.jappgeo.2013.03.014.

Campbell, M., Callow, J.N., McGrath, G., McGowan, H., 2017. A multimethod approach to inform epikarst drip discharge modelling: Implications for palaeo-climate reconstruction. Hydrol. Process. 31 (26), 4734–4747. https://doi.org/10.1002/hyp.11392.

Chalikakis, K., Plagnes, V., Guerin, R., Valois, R., Bosch, F.P., 2011. Contribution of geophysical methods to karst-system exploration: an overview. Hydrogeol. J. 19 (6), 1169–1180. https://doi.org/10.1007/s10040-011-0746-x.

Charles, S.P., Silberstein, R., Teng, J., Fu, G., Hodgson, G., Gabrovsek, C., Crute, J., Chiew, F.H.S., Smith, I.N., Kirono, D.G.C., Bathols, J.M., Li, L.T., Yang, A., Donohue, R.J., Marvanek, S.P., McVicar, T.R., Van Niel, T.G., Cai, W., 2010. Climate analyses for south-west Western Australia. A report to the Australian Government from the CSIRO South-West Western Australia Sustainable Yields Project. CSIRO, Australia. pp. 83.

Daily, W., Ramirez, A., LaBrecque, D., Nitao, J., 1992. Electrical resistivity tomography of vadose water movement. Water Resour. Res. 28 (5), 1429–1442. https://doi.org/10.1029/91WR03087.

Fohlmeister, J., Scholz, D., Kromer, B., Mangini, A., 2011. Modelling carbon isotopes of carbonates in cave drip water. Geochim. Cosmochim. Acta 75 (18), 5219–5228. https://doi.org/10.1016/j.gca.2011.06.023.

Ford, D., Williams, P.D., 2007. Karst Hydrogeology and Geomorphology. Wiley, Hoboken.

Gautam, P., Pant, S.R. Ando, H., 2000. Mapping of subsurface karst structure with gamma ray and electrical resistivity profiles: a case study from Pokhara valley, central Nepal. J. Appl. Geophys., 45/2: 97-110. https://doi.org/10.1002/9781118684986 Geotest user manual 2.50, Available from: http://www.geophysik-dr-rauen.de. Nov 2019.

Goldscheider, N. 2015. Overview of Methods Applied in Karst Hydrogeology. In Karst Aquifers—Characterization and Engineering; Springer International Publishing: New York, NY, USA, 2015; pp. 127–145.

Goldscheider, N., Meiman, J., Pronk, M., Smart, C., 2008. Tracer tests in karst hydrogeology and speleology. Int. J. Speleol. 37 (1), 27–40. https://doi.org/10.5038/1827-806X.37.1.3.

Grimes, K.G., 2006. Syngenetic karst in Australia: a review. Helictite 39 (2), 27–38.

Hall, G.J., Marnham, J.R., 2002. Regolith-landform Resources of the Karridale-tooker and Leeuwin 1:50000 Sheets. Dept. of Mineral and Petroleum Resources, Geological Survey of Western Australia, Perth, pp. 74.

Hartmann, A., Barberá, J.a., Lange, J, Andreo, B and Weiler, M. 2013. Progress in the hydrologic simulation of time variant recharge areas of karst systems – exemplified at a karst spring in Southern Spain. Adv. Water Resources, 54: 149-160. Doi: 10.1016/j.advwatres.2013.01.010.

Jennings, J., 1968. Syngenetic karst in Australia. In: Contributions to the study of karst, Willliams, P. M., Jennings, J. N. (Eds.), Research School of Pacific Studies, Australian National University special publication 6/5, Canberra, 1968.

Keshavarzi, M., Baker, A., Andersen, M.S., Kelly, B.J., 2017. River-groundwater connectivity in a karst system, Wellington, NSW, Australia. Hydrogeol. J. 25 (2), 557–574. https://doi.org/10.1007/s10040-016-1491-y.

Leopold, M., Völkel, J., Huber, J., Dethier, D., 2013. Subsurface architecture of the Boulder Creek Critical Zone Observatory from electrical resistivity tomography. Earth Surf. Proc. Land. 38 (12), 1417–1431. https://doi.org/10.1002/esp.3420.

Lipar, M., Webb, J.A., 2015. The formation of the pinnacle karst in Pleistocene aeolian calcarenites (Tamala Limestone) in southwestern Australia. Earth Sci. Rev. 140, 182–202. https://doi.org/10.1016/j.earscirev.2014.11.007.

Lipar, M., Webb, J.A., 2014. Middle–late Pleistocene and Holocene chronostratigraphy and climate history of the Tamala Limestone, Cooloongup and Safety Bay Sands, Nambung National Park, southwestern Western Australia. Aust. J. Earth Sci. 61 (8), 1023–1039. https://doi.org/10.1080/08120099.2014.966322.

Lippmann, E., 2008. 4 Point light 10W, Technical Data Operating Instructions Version 4.19. Available from: <http://www.l-gm.de>. 26.07.2020.

Loke, M.H., Dahlin, T., Rucker, D.F., 2014. Smoothness-constrained time-lapse inversion of data from 3D resistivity surveys. Near Surf. Geophys. 12, 5–24. https://doi.org/10.3997/1873-0604.2013025.

Lowe, M., McGrath, G., Mathes, F., Leopold, M., 2017. Evaluation of surfactant effectiveness on water repellent soils using electrical resistivity tomography. Agric. Water Manag. 181, 56–65. https://doi.org/10.1016/j.agwat.2016.11.013.

Mahmud, K., Mariethoz, G., Baker, A., Treble, P.C., 2018. Hydrological characterization of cave drip waters in a porous limestone: Golgotha Cave, Western Australia. Hydrol. Earth Syst. Sci. 22, 977–988. https://doi.org/10.5194/hess-22-977-2018.

Mahmud, K., Mariethoz, G., Baker, A., Treble, P.C., Markowska, M., McGuire, E., 2016. Estimation of deep infiltration in unsaturated limestone environments using cave lidar and drip count data. Hydrol. Earth Syst. Sci. 20 (1), 359–373. https://doi.org/10.5194/hess-20-359-2016.

Mahmud, K., Mariethoz, G., Treble, P., Baker, A., 2015. Terrestrial Lidar Survey and Morphological Analysis to Identify Infiltration Properties in the Tamala Limestone, Western Australia, Selected Topics in Applied Earth Observations and Remote Sensing. IEEE J. 8 (10), 4871–4881. https://doi:10.1109/JSTARS.2015.2451088.

Michot, D., Benderitter, Y., Dorigny, A., Nicoullaud, B., King, D., Tabbagh, A., 2003. Spatial and temporal monitoring of soil water content with an irrigated corn crop cover using surface electrical resistivity tomography. Water Resour. Res. 39/5 https://doi.org/10.1029/2002WR001581.

Pakzad, L., Ein-Mozaffari, F., Chan, P., 2008. Using electrical resistance tomography and computational fluid dynamics modelling to study the formation of cavern in the mixing of pseudoplastic fluids possessing yield stress. Chem. Eng. Sci. 63 (9), 2508–2522. https://doi.org/10.1016/j.ces.2008.02.009.

Park, M.K., Park, S., Yi, M.J., Kim, C., Son, J.S., Kim, J.H., Abraham, A.A., 2014. Application of electrical resistivity tomography (ERT) technique to detect underground cavities in a karst area of South Korea. Environ. Earth Sci. 71 (6), 2797–2806. https://doi.org/10.1007/s12665-013-2658-7.

Putiška, R., Nikolaj, M., Dostál, I., Kušnirák, D., 2012. Determination of cavities using electrical resistivity tomography. Contribut. Geophys. Geodesy 42 (2), 201–211. https://doi.org/10.2478/v10126-012-0018-3.

Raupach, M.R., Briggs, P.R., Haverd, V., King, E.A., Paget, M., Trudinger, C.M., 2011. Australian Water Availability Project. CSIRO Marine and Atmospheric Research, Canberra, Australia.

Robert, T., Dassargues, A., Brouyère, S., Kaufmann, O., Hallet, V., Nguyen, F., 2011. Assessing the contribution of electrical resistivity tomography (ERT) and self-potential (SP) methods for a water well drilling program in fractured/karstified limestones. J. Appl. Geophys. 75 (1), 42–53. https://doi.org/10.1016/j.jappgeo.2011.06.008.

Samouëlian, A., Cousin, I., Tabbagh, A., Bruand, A., Richard, G., 2005. Electrical resistivity survey in soil science: a review. Soil Tillage Res. 83 (2), 173–193. https://doi.org/10.1016/j.still.2004.10.004.

Tapsell, P., Newsome, D., Bastian, L., 2003. Origin of yellow sand from Tamala limestone on the Swan Coastal Plain, Western Australia. Aust. J. Earth Sci. 50 (3), 331–342. https://doi.org/10.1046/j.1440-0952.2003.00989.x.

Treble, P.C., Fairchild, I.J., Baker, A., Meredith, K.T., Andersen, M.S., Salmon, S.U., Bradley, C., Wynn, P.M., Hankin, S., Wood, A., McGuire, E., 2016. Roles of forest bioproductivity, transpiration and fire in a nine-year record of cave dripwater chemistry from southwest Australia. Geochim. Cosmochim. Acta 184, 132–150. https://doi.org/10.1016/j.gca.2016.04.017.

Treble, P.C., Fairchild, I.J., Griffiths, A., Baker, A., Meredith, K.T., Wood, A., McGuire, E., 2015. Impacts of cave air ventilation and in-cave prior calcite precipitation on Golgotha Cave dripwater chemistry, southwest Australia. Quat. Sci. Rev. 127/, 61–72. https://doi.org/10.1016/j.quascirev.2015.06.00.

Treble, P.C., Bradley, C., Wood, A., Baker, A., Jex, C.N., Fairchild, I.J., Gagan, M.K., Cowley, J., Azcurra, C., 2013. An isotopic and modelling study of flow paths and storage in Quaternary calcarenite, SW Australia: implications for speleothem paleoclimate records. Quat. Sci. Rev. 64, 90–103. https://doi.org/10.1016/j.quascirev.2012.12.015.

Vacher, H.L., Mylroie, J.E., 2002. Eogenetic karst from the perspective of an equivalent porous medium. Carbonates Evaporites 17 (2), 182–196. https://doi.org/10.1007/BF03176484.

Valois, R., Bermejo, L., Guérin, R., Hinguant, S., Pigeaud, R., Rodet, J., 2010. Karstic morphologies identified with geophysics around Saulges caves (Mayenne, France). Archaeol. Prospect. 17, 151–160. https://doi.org/10.1002/arp.385.

Vanderborght, J., Kemna, A., Hardelauf, H., Vereecken, H., 2005. Potential of electrical resistivity tomography to infer aquifer transport characteristics from tracer studies: A synthetic case study. Water Resour. Res. 41/6 https://doi.org/10.1029/2004WR003774.

Viney, N., J. Vaze, R., Crosbie, B., Wang, W., Dawes, A., Frost, 2015. AWRA-L v5. 0: Technical description of model algorithms and inputs. http://www.bom.gov.au/water/landscape/static/publications/Viney_et_al_2015_AWRA_L_5.0_model_description.pdf.

Watlet, A., Kaufmann, O., Triantafyllou, A., Poulain, A., Chambers, J.E., Meldrum, P.I., Wilkinson, P.B., Hallet, V., Quinif, Y., Van Ruymbeke, M., Van Camp, M., 2018. Imaging groundwater infiltration dynamics in the karst vadose zone with long-term ERT monitoring. Hydrol. Earth Syst. Sci. 22, 1563–1592. https://doi.org/10.5194/hess-22-1563-2018.

Williams, P.W., 1983. The role of the subcutaneous zone in karst hydrology. J. Hydrol. 61, 45–67. https://doi.org/10.1016/0022-1694(83)90234-2.

Yamada, M., Ohsawa, S., Matsuoka, H., Watanabe, Y., Brahmantyo, B., Maryunani, K.A., Tagami, T., Kitaoka, K., Takemura, K., Yoden, S., 2008. Derivation of travel time of

limestone cave drip water using tritium/helium 3 dating method. Geophys. Res. Lett. 35, L08405. https://doi.org/10.1029/2008GL033237.

Zenone, T., Morelli, G., Teobaldelli, M., Fischanger, F., Matteucci, M., Sordini, M., Armani, A., Ferrè, C., Chiti, T., Seufert, G., 2008. Preliminary use of ground-penetrating radar and electrical resistivity tomography to study tree roots in pine forests and poplar plantations. Funct. Plant Biol. 35 (10), 1047–1058. https://doi.org/10.1071/FP08062.

Zhou, W., Beck, B.F., Adams, A.L., 2002. Effective electrode array in mapping karst hazards in electrical resistivity tomography. Environ. Geol. 42 (8), 922–928. https://doi.org/10.1007/s00254-002-0594-z.